

RESEARCH ARTICLE

An inkjet-printed bendable antenna for wearable electronics

Hang Yu^{1,2†}, Xingguo Zhang^{1†}, Hao Zheng¹, Dachao Li¹, Zhihua Pu^{1*}¹State Key Laboratory of Precision Measuring Technology and Instruments, Tianjin University, Tianjin, China²School of Instrumentation and Optoelectronic Engineering, Beihang University, Beijing, China

Abstract

Flexible antennas, which can conform to the skin and transfer signals to terminals, are particularly useful for wearable electronics. Bending, which frequently occurs to flexible devices, significantly affects the performance of flexible antennas. Inkjet printing has been used as an additive manufacturing technology for fabricating flexible antenna in recent years. However, there is little research on the bending performance of inkjet printing antenna in both simulation and experiment. This paper proposes a bendable coplanar waveguide antenna with a small size of $30 \times 30 \times 0.05 \text{ mm}^3$ by combining the advantages of fractal antenna and serpentine antenna, which realizes the ultra-wideband feature and avoids the problems of large dielectric layer thickness (greater than 1 mm) and large volume of traditional microstrip antenna at the same time. The structure of the antenna was optimized by simulation using the Ansys high-frequency structure simulator, and the antenna was fabricated on a flexible polyimide substrate by inkjet printing. The experimental characterization results show that the central frequency of the antenna is 2.5 GHz, the return loss is -32 dB , and the absolute bandwidth is 850 MHz, which is consistent with the simulation results. The results demonstrate that the antenna has anti-interference capability and can meet the ultra-wideband characteristics. When the traverse and longitudinal bending radius are greater than 30 mm and skin proximity greater than 1 mm, the resonance frequency offsets are mostly within 360 MHz, and return losses of the bendable antenna are within the -14 dB compared with the no bending condition. The results exhibit that the proposed inkjet-printed flexible antenna is bendable and promising for wearable applications.

[†]These authors contributed equally to this work.

***Corresponding author:**
Zhihua Pu (puzhihua@tju.edu.cn)

Citation: Yu H, Zhang X, Zheng H, *et al.*, 2023, An inkjet-printed bendable antenna for wearable electronics. *Int J Bioprint*. <https://doi.org/10.18063/ijb.722>

Received: December 27, 2022

Accepted: February 07, 2023

Published Online: March 29, 2023

Copyright: © 2023 Author(s). This is an Open Access article distributed under the terms of the Creative Commons Attribution License, permitting distribution and reproduction in any medium, provided the original work is properly cited.

Publisher's Note: Whioce Publishing remains neutral with regard to jurisdictional claims in published maps and institutional affiliations.

Keywords: Flexible antenna; Bendable antenna; Coplanar waveguides; Inkjet printing

1. Introduction

Flexible wearable electronics is a research hotspot in the biomedical field^[1-6], and a flexible antenna that can conform to the skin is a critical component^[7,8]. Flexible antenna can be used for communication between electronic devices attached to the outer surface of human skin and personal wireless terminals^[9,10]. With the advent of 5G technology, the rapid development of wireless communication technology, and the increasingly extensive application of wearable devices in daily life, there are stricter requirements

for wireless communication systems based on antenna structures and small sensors^[11,12]. The development of electronic devices is trending toward miniaturization, portability, and intelligence, especially in the field of wearable electronics^[13,14]. Therefore, in order to meet the developing needs of communication and information technology, researches on mobile and flexible antennas have been gaining interest. The recent research on flexible antenna mainly focuses on the antenna structure design and the methods of manufacturing flexible antenna.

For antennal structure design, it is required to meet the requirements of compact, multiband and broadband structure design simultaneously to adapt to the trend of modern communication system integration and wearability. In particular, the wideband flexible antennas, which have wider impedance bandwidth, can achieve higher data transmission rates and enable vast applications. Sahnoun *et al.* designed an ultra-wideband (UWB) flexible monopole antenna integrated with a narrow-band rectangular slot^[15]. The results showed that the monopole antenna covers an UWB from 2 to 12 GHz with S_{11} less than -10 dB. Hasan *et al.* proposed a coplanar waveguide (CPW)-fed flexible antenna with a circular patch^[16], which has UWB performance and a bandwidth ratio of 188.5%. Jayshri Kulkarni *et al.* fabricated a wideband CPW-fed monopole antenna for Wi-Fi5 and Wi-Fi6 applications^[17]. The measured wideband operation of 34.5% (5.15–7.29 GHz) is obtained by a single resonance at 6.2 GHz, conforming to the bandwidth requirement of Wi-Fi5 and Wi-Fi6. However, these papers did not consider the influence of bending on the antennas.

There are two common ways to manufacture flexible antennas. One of the methods is to use flexible fabric as the substrate and use bonding or embroidery to make flexible antennas, while the other is printing technology used to prepare flexible antennas on a flexible substrate. The latter has a mature production mode and excellent antenna performance, and allows for easy mass production. Printing technology includes screen printing^[18], 3D printing^[19], and inkjet printing^[20]. Inkjet printing has the merit of direct writing and involving no mask, which is widely used in the manufacturing of flexible antennas. Jilani *et al.* proposed an inkjet-printed millimeter-wave flexible antenna based on a polyethylene terephthalate substrate for 5G wireless applications^[20]. The prototype exhibited an impedance bandwidth of 26–40 GHz, a consistent omnidirectional radiation pattern, and a peak gain of 7.44 dBi at 39 GHz.

On the other hand, inkjet-printed CPW-fed bendable antenna has also been explored through research. Guo *et al.* demonstrated a fully printed CPW-fed antenna based on silver-nanoparticles on the polyethylene terephthalate

substrate. The radiating properties of the antenna were investigated. The simulated and measured reflection coefficients are ~ -31 dB and ~ -23 dB, respectively. Meanwhile, the -10 dB bandwidth is ~ 530 MHz and the obtained VSWR is ~ 1.3 . Radiating properties were characterized and agreed well with the simulation results^[21]. Hettak *et al.* investigated an inkjet-printed millimeter-wave antenna on polyethylene terephthalate (PET) substrate. The 60 GHz CPW-fed monopole antenna was printed with a DMP-2800 series inkjet printing system. The measured impedance bandwidth of the printed antenna, defined by return loss of less than -10 dB, is from 60 to 65 GHz^[22]. However, in the structural design, it is not possible to obtain UWB features while avoiding large dielectric layer thickness and volume at the same time. In addition, the effect of the simulation and experiment on the bending of these previous works has not been studied yet, especially under different bending curvatures.

This paper proposes a bendable antenna based on inkjet printing silver nanoparticles. The bendable antenna is designed with a center frequency at 2.45 GHz and presented a CPW structure with a small size of $30 \times 30 \times 0.05$ mm³, making it convenient to integrate with flexible wearable electronics and detect the real-time and efficient transmission of epidermis information. By contrasting performance results based on electromagnetic field simulations using Ansys high-frequency structure simulator (HFSS), the prototype of the flexible low-profile antenna was obtained. Furthermore, the bendable antenna was fabricated by inkjet printing on flexible polyimide substrate, and its stability was verified using various measurement setups and performance tests.

2. Materials and methods

2.1. Antenna structure and models

A planar structure is helpful to improve the stability of the antenna and enlarge the scope of effective work. The resonant frequency of the antenna depends on the electrical length of the antenna. The larger the electrical length, the lower the resonant frequency. The single-frequency and multifrequency characteristics of the antenna are determined by the symmetry of the antenna vibrator, and the vibrator branches with different lengths can produce different resonance frequencies. The designed low-profile flexible antenna with a center frequency of 2.45 GHz determines the complete symmetry of the two arms of the dipolar oscillator. The input impedance of the antenna depends on its length, width, structure layout, feeding position, and mode, while the return loss depends on the matching degree of the antenna impedance, that is, the pure resistance of the input impedance and the proximity to the characteristic impedance of the transmission line.

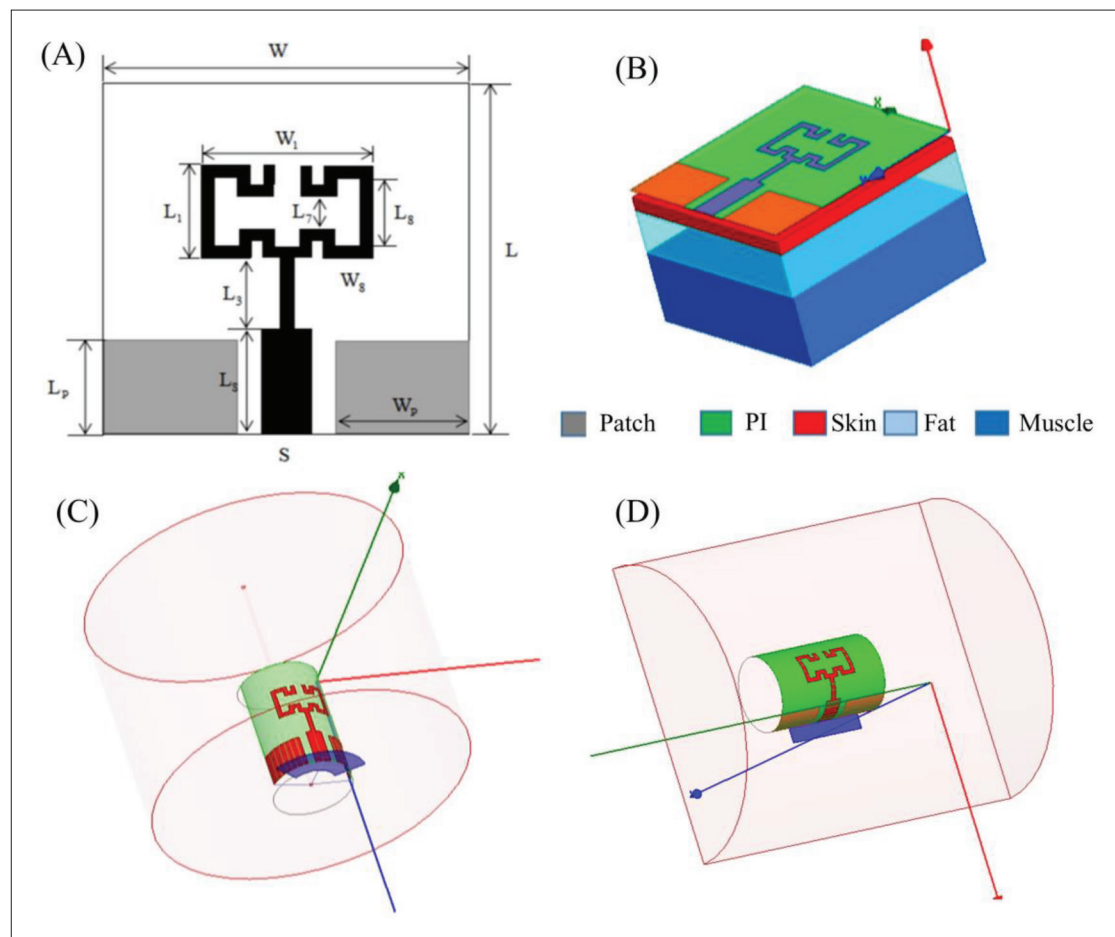


Figure 1. Antenna structure and models. (A) Antenna configuration. (B) Three-layered rectangular phantom. (C) Transverse bending phantom. (D) Longitudinal bending phantom.

For the UWB characteristics and low-profile structure of the antenna, high performance can be achieved by CPW feeding, which is widely applicable to the design of flexible printed circuits^[23,24].

The flexible antenna structure and models used in this study are shown in Figure 1A. In this work, we designed the vibrator with a symmetric bifurcation structure and the feed end with a CPW structure, which enables the UWB feature^[25] and reduces the volume and thickness (less than 1 mm) compared with the conventional microstrip antenna dielectric layers, thus providing a low profile and high flexibility. The proposed structure was modeled and simulated using the HFSS tool, and the input impedance, return loss, field distribution, gain, and other performance parameters were obtained. Based on the simulation, the frequency was swept and the results were analyzed to obtain the optimal size parameters of the antenna, which are expressed as follows: total length (L) = 30 mm, total width (W) = 30 mm, thickness of the substrate (h) = 0.05 mm, area of the ground patch (L_p) = 8 mm, W_p = 11 mm, area

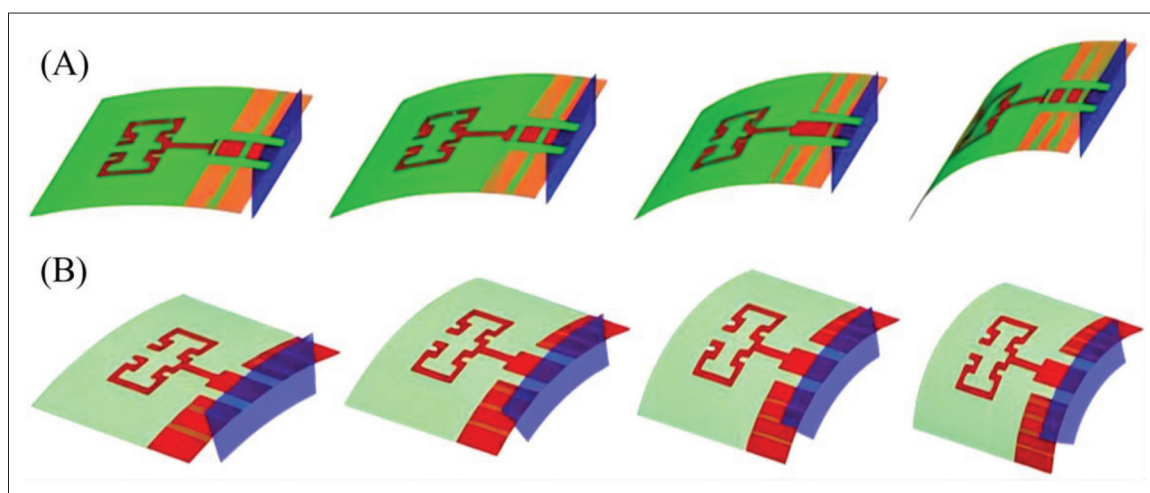
of the central conductor patch (L_s) = 9 mm, L_3 = 6 mm, L_1 = 8 mm, W_1 = 14 mm, and width of the antenna feeder (S) = 4 mm. In order to increase the effective electrical length of the radiation patch, a slot was made in the middle of the patch, and the size of the hollow part is L_8 = 6 mm, W_8 = 2 mm, L_7 = 3 mm.

In addition, to determine the reliability of the antenna performance under wearable conditions, the conformal ability of the antenna and the influence of human tissue on the antenna performance were evaluated. A three-layer cubical tissue model was designed in the simulation, as shown in Figure 1B. The tissue model includes skin (2 mm thick), fat (10 mm thick), and muscle layers (28 mm thick)^[27], which were used to analyze the influence of different spacing distances on antenna return loss. The specific parameters of the three-layer tissue model are shown in Table 1.

In practice, although there is complex bending deformation including symmetrical and asymmetry

Table 1. Human tissue model parameters at 2.45 GHz^[26]

Body tissue	Skin	Fat	Muscle
Relative dielectric constant	38.007	5.280	52.729
Dielectric loss angle	0.283	0.145	0.241
Magnetic conductivity (s/m)	1.49	0.11	1.77
Thickness (mm)	2	10	28

**Figure 2.** Antenna conformal models. (A) Antenna longitudinal bending models (bending radius = 70 mm, 55 mm, 40 mm, 25 mm, respectively). (B) Antenna transverse bending models (bending radius = 70 mm, 40 mm, 25 mm, 20 mm, respectively).

deformations, complex bending deformations can be decomposed into components in two directions: longitudinal and transverse components. Hence, in this study, we investigated the symmetrical deformations. More complex deformation in real applications will be studied and transformed into symmetric deformation in future research. The effective conformal operation and curve modeling methods are shown in Figure 1C and D. In HFSS, an ideal cylinder model with a certain degree of curvature can be constructed, and the antenna can be attached layer by layer using the “Wrap Sheets.” The substrate was thickened by “thick sheet”; the media entity was created; the region was wrapped, the synthetic radiation patch was united; the engineering variable r of the radius was created; and its parameters were scanned. The transverse and longitudinal bending with different curvatures (bending radius from 70 to 20 mm) of the conformal antenna model was established to generate a different bending degree of the antenna model, and the electric performance parameters were analyzed, as shown in Figure 2A and B.

2.2. Antenna processing and measurement setup

Polyimide film (0.05 mm thick) was used as the flexible substrate for the antenna, and a silver coating was used as a radiation conductor. Silver nanoparticles were selected as the conductive material of the CPW-fed antenna because

the processing is simple. Conductive silver ink spots were deposited on the polyimide film surface to form the array of antennas^[28]. The finished product is shown in Figure 3A. In this process, the polyimide film was placed flat on the glass sheet.

The polyimide (PI) substrate was subject to purified water cleaning, ethanol cleaning, and hydrophilic treatment. The antenna's pattern was imported to the inkjet printer through the computer. The silver nanoparticles (bought from Sigma-Aldrich) were fabricated by an inkjet printer system (Microfab Jetlab®II)^[29] at 90°C heating conditions. In addition, the accuracy of this inkjet printing system was 5 μm in X and Y directions, so different printing runs have high repeatability and slight deviation. After inkjet printing silver nanoparticles, the antenna was sintered at 250°C for 2 h for annealing and removing the organic solvent in ink. In addition, the printed electrodes have a thickness of approximately 800–1000 nm.

As shown in Figure 3B and C, the antenna feed end was fixed and connected with the port of the SubMiniature version A (SMA) using conductive silver paste, which was connected to the Agilent E5072A network analyzer through a 50 Ω coaxial transmission line. Figure 3D–F show the test setup for the antenna bending condition, and Figure 3G shows the measurement setup for the human

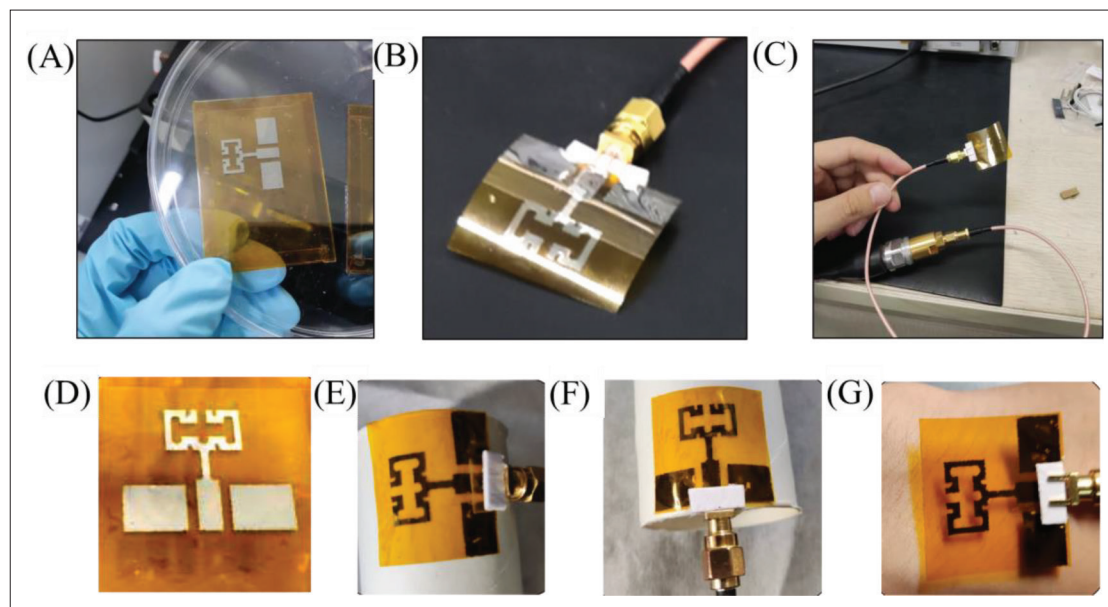


Figure 3. Antenna processing and measurement setup. (A,B) Antenna based on inkjet printing. (C) Antenna connected with SMA port. (D) Antenna in planar condition. (E) Antenna in longitudinal bending condition. (F) Antenna in transverse bending condition. (G) Measurement setup for human body and antenna effects.

body and antenna effects. The conformal surface used highly insulated noncoated paper, and the human body tissue used the flat arm area.

3. Results and discussion

3.1. Simulation results of bendable antenna performance

Figure 4A shows the electric field distribution of the antenna, which is concentrated at $0-6 \times 10^3$ V/m. The direction of the electric field line is different from the excitation end to the divergence end. Along the direction of the antenna electric length, the change of the field strength presents a sine and cosine distribution, but along the direction of the ground and feeder line width, the electric field distribution presents a saddle-type distribution. At the gap between the antenna feeder and ground, the direction of the electric field intensity is opposite, and the difference is the largest.

As shown in Figure 4B, based on the analysis of the Smith chart, the marker point at M1 is close to the geometric center point of the circle diagram. The input impedance is $(46.15 + 0.58j) \Omega$, showing pure resistance characteristics of 46.15Ω and a small inductive reactance value, which means that the antenna has a good “impedance match” and “return loss” at 2.45 GHz, where the antenna radiation efficiency is high. With the frequency sweep from 2 to 3 GHz, the visible point moves from M2 to M3, approaching the center first and then moving away from the center in the circle graph, indicating that the reflection loss decreases first and then increases. If the frequency

sweep range is enlarged, the intersecting and receding spiral lines can be obtained.

Simulation results of antenna electrical parameters are shown in Figure 4C and D. The center frequency of the bendable antenna is 2.45 GHz and the return loss at the resonant point reaches -28 dB. The lower limit frequency f_L is 2.16 GHz, the upper limit frequency f_H is about 2.8 GHz, and the absolute bandwidth reaches 640 MHz. The equivalent input impedance of the antenna is $(46.45 + 0.61j) \Omega$, which is close to the ideal pure resistance of 50Ω .

As shown in Figure 4E and F, the far-field gain plot of antenna planes E and H were obtained by simulation. The radiation power of plane E diverges evenly from the center to all sides, and the radiation power of plane H resembles the shape of figure “eight.” The overall 3D gain exhibits dipole characteristics. To evaluate the radiation safety of the antenna, based on the analysis of the three-layer human tissue model in Figure 4G, the specific absorption rate (SAR) distribution on the skin surface was determined, as presented in Figure 4H. The results show that, in the simulation of human tissue, the SAR was lower than the standard value of 1.6 W/kg in all locations, indicating that the radiation is not harmful to the human body.

3.2. Simulation of bendable antenna conformal performance

Figure 5A shows the S-parameter curve based on the various curvatures radius in the longitudinal direction at 2.45 GHz, indicating the approximate trend of its

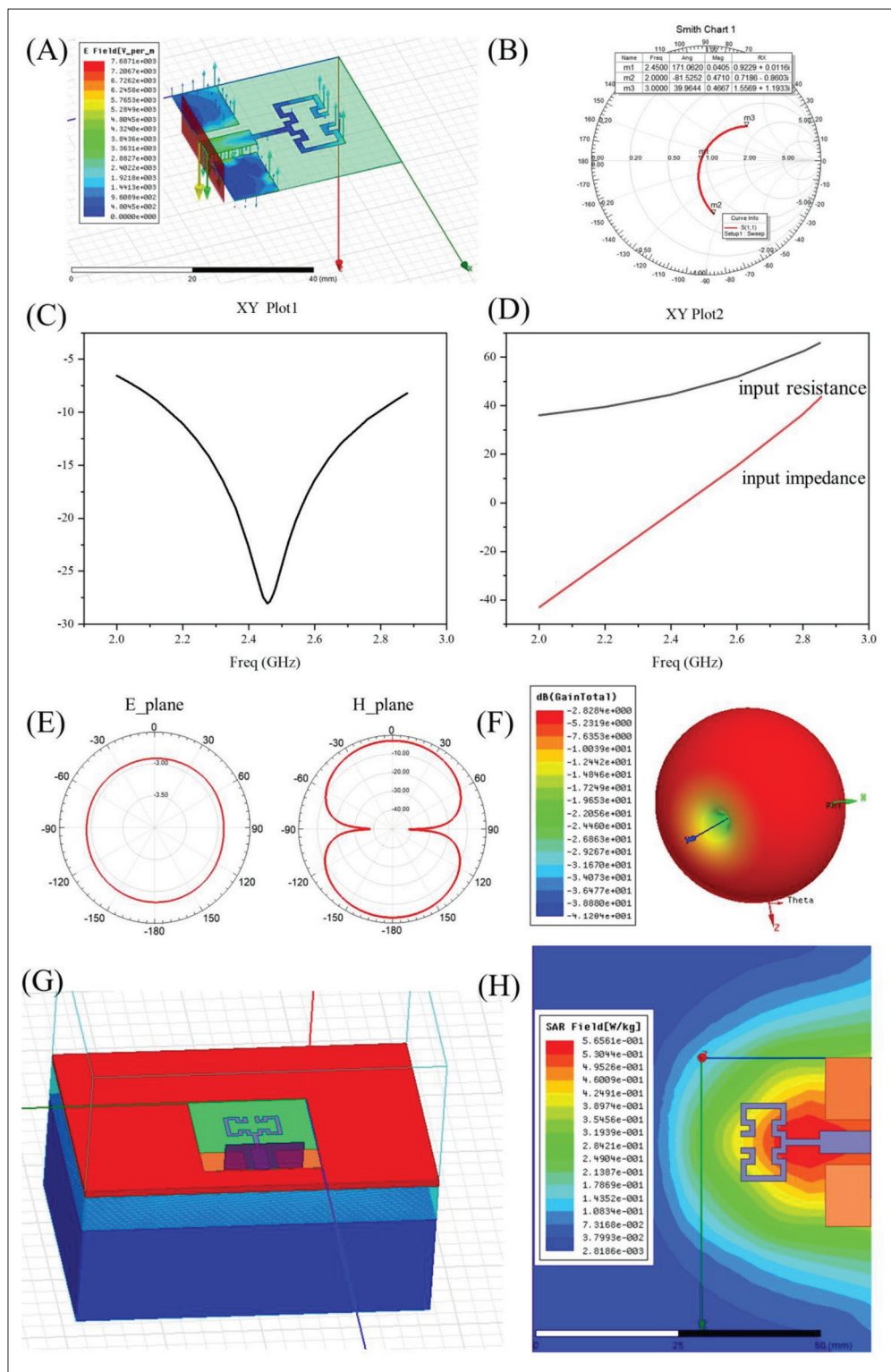


Figure 4. Simulation results of antenna performance. (A) Antenna electric field distribution. (B) Smith chart. (C) Return loss plot of antenna. (D) Input impedance plot of antenna. (E) Gain pattern of the proposed antenna in E-plane and H-plane. (F) Gain in 3D model. (G) Three-layer body tissue model in simulation. (H) Specific absorption rate for the antenna.

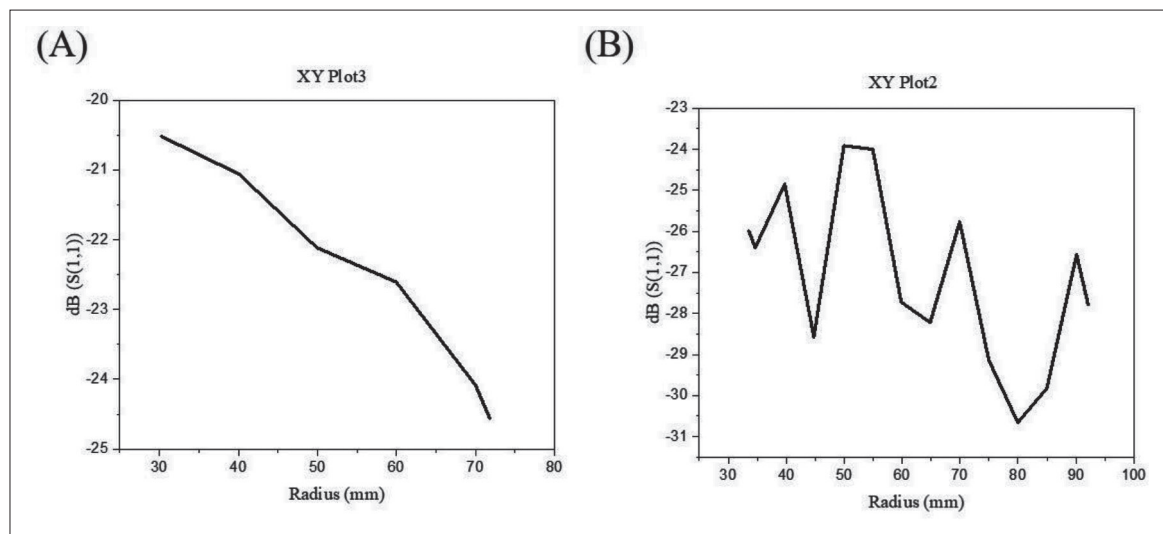


Figure 5. Simulation of antenna conformal performance. (A) S_{11} is changed by various curvatures of the antenna in longitudinal bending conditions. (B) S_{11} is changed by various curvatures of the antenna in transverse bending conditions.

return loss as a function of the degree of bending. The bending of the antenna in the length direction changes the meandering trend. The greater the degree of bending deformation, the greater the electrical length. The longitudinal bending causes a slight increase in the length of the dimension. A slight increase in the electrical length causes a corresponding decrease of the resonant frequency, and the equivalent input impedance changes at the same time, thus altering the return loss.

Figure 5B shows the S-parameter curve based on the various curvature radius in the transverse direction at 2.45 GHz. In the width direction, it can be seen that its return loss changes irregularly with the degree of bending. The change of the antenna trace width does not change the direction of the meander. The bend in the width direction will not only change the electrical length and grounding width of the trace slightly but also change the size of the feed gap, and thus, the equivalent input impedance changes irregularly.

3.3. Measurement results of bendable antenna performance

In the experiment, adjusting the curvature of the conformal plane (the curvature changed from plane to curvature radius = 30 mm) and the distance (distance increases from 2 to 8 mm) between the antenna and the skin tissue to measure the electrical properties in the cases of no bending, transverse bending, and longitudinal bending, and to examine the effect of proximity to the skin (the distance is greater than 1 mm). The results consist of the Smith chart, return loss, and frequency characteristics of each state.

In the experimental test, as shown in Figure 6A, the antenna center frequency obtained by the network analyzer

is 2.5 GHz, the return loss at the resonant point is -32 dB, the lower limit frequency f_L of the antenna's -10 dB cut-off interval is about 2 GHz, and the upper limit frequency f_H is about 2.85 GHz under the condition of no bending. The absolute bandwidth is about 850 MHz, which meets the UWB characteristics. Under these conditions, the measured center frequency is larger than the simulation, the effective bandwidth is larger, and the curves are uneven and wobbly.

The experimental results are relatively close to the simulations, but there are some minor deviations. The center of the measured frequency is larger than the simulation, but the measured return loss is lower. The measured curve is not smooth due to the inhomogeneity of inkjet printing, the coupling effect of the environment on the antenna and the inevitable errors in the antenna welding process, and the asymmetry of feed may cause multiple frequency points to spike, so the waveform does not appear smooth. In future research, impedance matching can be optimized to reduce antenna radiation loss.

According to Figure 6B and Table 2, when the radius of curvature decreases gradually in the transverse and longitudinal bending conditions, the center frequency continuously shifts to the low-frequency direction with the increased longitudinal bending degree (the curvature radius = plane, 70 mm, 60 mm, 50 mm, 40 mm, 30 mm, and 15 mm, respectively), and the return loss increases gradually as the S-parameter curve rises.

According to Figure 6C, as the transverse bending of the antenna increases (the curvature radius = plane, 70 mm, 60 mm, 50 mm, 40 mm, and 30 mm, respectively), the return loss tends to increase slightly. The transverse

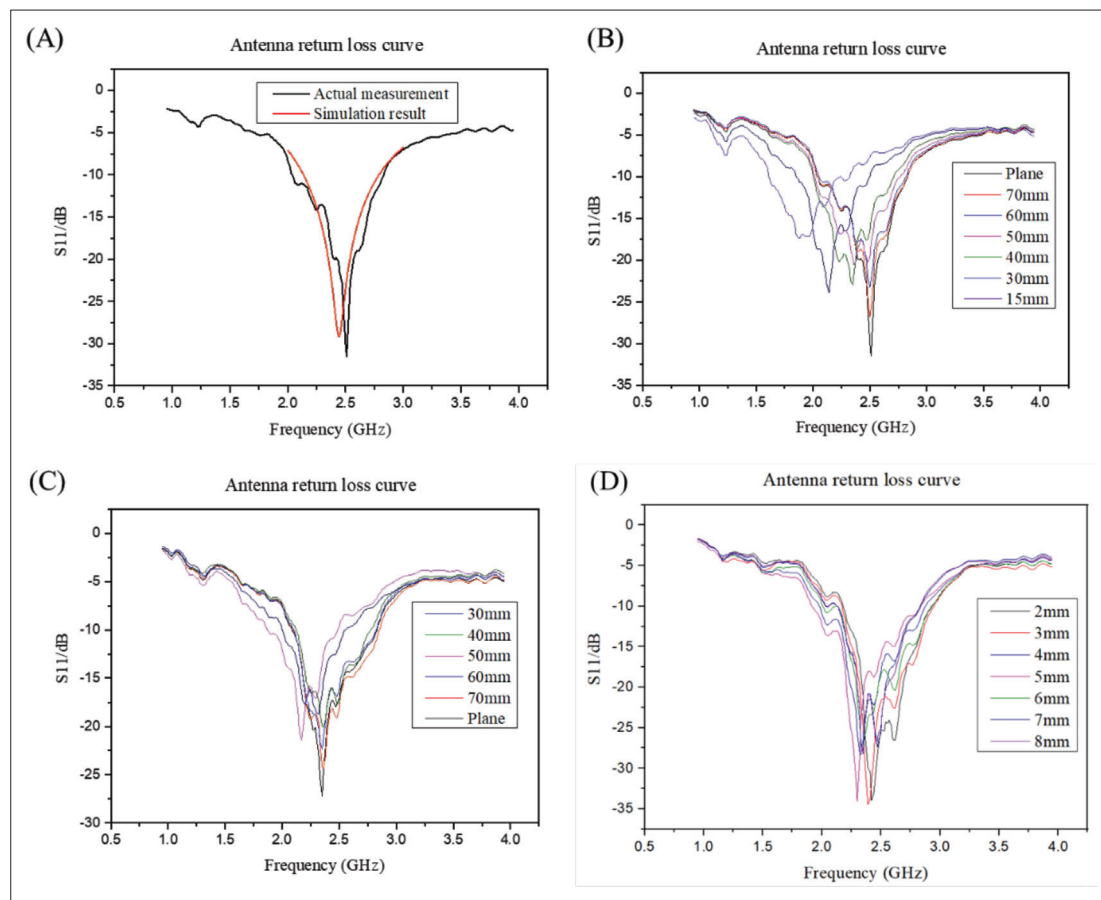


Figure 6. Measured results of antenna performance. (A) Comparison for S_{11} between the antenna simulation and test. (B) S_{11} plot for the antenna in transverse bending condition. (C) S_{11} plot for antenna in longitudinal bending condition. (D) S_{11} plot for human body and antenna effects.

Table 2. Comparison of center frequency and return loss in three situations

Bending curvature radius	Center frequency (GHz)	Return loss (dB)	Center frequency (GHz)	Return loss (dB)	Distance between antenna and skin tissue	Center frequency (GHz)	Return loss (dB)
	In transverse bending condition		In longitudinal bending condition			For human body and antenna effects	
Plane	2.51	-31.5	2.35	-27.2	2 mm	2.42	-34.0
70 mm	2.50	-26.8	2.36	-24.4	3 mm	2.39	-34.4
60 mm	2.50	-23.2	2.35	-22.3	4 mm	2.33	-28.3
50 mm	2.36	-20.6	2.17	-21.4	5 mm	2.30	-34.1
40 mm	2.35	-23.0	2.36	-20.1	6 mm	2.35	-27.8
30 mm	2.14	-23.9	2.32	-18.7	7 mm	2.35	-27.7
15 mm	1.88	-17.4			8 mm	2.35	-28.2

bending of the radiating conductor has no significant effect on the antenna center frequency or power loss. However, when the bending degree is high, the bending of the central conductor band induces coupling and makes the antenna performance abrupt.

The electromagnetic wave has a high frequency and short wavelength, and when it irradiates the skin tissue,

the conductive biological components will affect the antenna's performance. Figure 6D shows the changing antenna return loss when the skin is close to the antenna radiation patch (the distance is still greater than 1 mm). When the distance between them increases (2–8 mm), the center frequency of the antenna varies slightly, and the S_{11} curve exhibits slight shifts up and down. These differences

Table 3. Comparison of the current study and previous works

References no.	Antenna type	Dimensions	Fabrication method	Substrate	Bandwidth	Performance under bending
[15]	Integrated UWB/narrow-band antenna	$63.6 \times 37 \times 0.254 \text{ mm}^3$	Printed	Rogers RO3003 substrate	2–12 GHz	Tested on a cylinder with a radius of curvature of 20 mm
[16]	CPW-fed	$81 \times 20 \text{ mm}^2$	Knitted	Fabric	—	The efficiency of flexible antenna under different stretching levels was tested
[17]	CPW-fed	$20 \times 8.7 \times 0.4 \text{ mm}^3$	Printed	FR-4	5.15–7.29 GHz	—
[20]	CPW-fed slotted monopole antenna	$12.8 \times 7.5 \times 0.135 \text{ mm}^3$	Inkjet printing	PET	26–40 GHz	—
[21]	CPW-fed	$40 \times 35 \times 0.3 \text{ mm}^3$	Inkjet printing	PET	The –10 dB bandwidth is ~530 MHz	The performance under 40 mm bending radius was tested
[22]	CPW-fed	$\sim 200 \times 300 \text{ mm}^2$	Inkjet printing	PET	60–65 GHz	—
Our work	Integrated the CPW-fed structure and the T-type fractal	$30 \times 30 \times 0.05 \text{ mm}^3$	Inkjet printing	PI	2–2.85 GHz	The influence of transverse bending and longitudinal bending with different curvatures on the performance was studied

Abbreviations: CPW, coplanar waveguide; PET, polyethylene terephthalate; PI, polyimide; UWB, ultra-wideband

may be related to the tissue density, which has a variable distribution. Overall, the resonance frequency offsets are mostly within 360 MHz and the return loss of the bendable antenna are within the –14 dB compared with the no bending condition. The performance variation meets the general requirements.

In addition, the comparison of this paper and previous other works is shown in Table 3. In short, in this work, we integrated fractal antenna and serpentine antenna based on the meander technology; achieved UWB feature and avoided large dielectric layer thickness and volume at the same time; fabricated the bending antenna by inkjet printing technology; and studied the influence of transverse bending and longitudinal bending with different curvature on the performance in simulation and experiments.

4. Conclusion

This paper proposes a new coplanar waveguide structure for bendable antennas by combining the advantages of fractal antenna and serpentine antenna, which realizes the UWB feature and avoids the problems of large dielectric layer thickness (greater than 1 mm) and large volume of traditional microstrip antenna at the same time. HFSS simulations were performed to obtain the optimal structure parameters, and the bendable antenna was fabricated at a low temperature by inkjet printing. Furthermore, the bendable performance of the antenna was evaluated. The results show that the central frequency of the antenna is 2.5 GHz, the return loss of the antenna

is –32 dB, and the absolute bandwidth of the antenna is 850 MHz, which are consistent with the simulation results. The results demonstrate that the antenna have anti-interference capability and can meet the characteristics of UWB. Regarding the bendable performance of the antenna, for traverse and longitudinal bending radii that are greater than 30 mm and skin proximity greater than 1 mm, the resonance frequency offsets are mostly within 360 MHz and return loss of the bendable antenna are within the –14 dB compared with the no bending condition, demonstrating robust performance in transmission. In conclusion, the designed bendable antenna provides an effective solution for wearable applications and next-generation 5G communications.

Acknowledgments

None.

Funding

This work was supported by the National Natural Science Foundation of China (No. 82102230), the National Key R&D Program of China (No. 2018YFE0205000), and the 111 Project of China (No. B07014).

Conflict of interest

The authors have no conflicts of interest.

Author contributions

Conceptualization: Zhihua Pu, Dachao Li

Investigation: Hang Yu, Xingguo Zhang

Methodology: Hang Yu, Hao Zheng

Writing – original draft: Hang Yu, Xingguo Zhang

Writing – review & editing: Xingguo Zhang, Zhihua Pu

Ethics approval and consent to participate

Not applicable.

Consent for publication

Not applicable.

Availability of data

Data are available from corresponding author on reasonable request.

References

- Kim Y, Oh JH, 2020, Recent progress in pressure sensors for wearable electronics: From design to applications. *Appl Sci Basel*, 10(18):6403.
- Spanu A, Casula G, Cosseddu P, *et al.*, 2021, Flexible and wearable monitoring systems for biomedical applications in organic flexible electronics: Fundamentals, devices, and applications, in *Organic Flexible Electronics*, Elsevier, 599–625.
- Wang L, Xu T, Fan C, *et al.*, 2021, Wearable strain sensor for real-time sweat volume monitoring. *iScience*, 24(1):102028.
- Wang LR, Xu TL, Zhang XJ, 2021, Multifunctional conductive hydrogel-based flexible wearable sensors. *Trends Anal Chem*, 134:116130.
- Pu Z, Zhang X, Yu H, *et al.*, 2021, A thermal activated and differential self-calibrated flexible epidermal biomicrofluidic device for wearable accurate blood glucose monitoring. *Sci Adv*, 7(5):eabd0199.
- Liu W, Xie RJ, Zhu JY, *et al.*, 2022, A temperature responsive adhesive hydrogel for fabrication of flexible electronic sensors. *NPJ Flex Electron*, 6(1):68.
- Gharbi El, Fernandez-Garcia MR, Ahyoud S, *et al.*, 2020, A review of flexible wearable antenna sensors: Design, fabrication methods, and applications. *Materials (Basel)*, 13(17):3781.
- Nappi S, Miozzi C, Mazzaracchio V, *et al.*, 2021, A plug&play flexible skin sensor for the wireless monitoring of pandemics, in *2021 IEEE International Conference on Flexible and Printable Sensors and Systems (FLEPS)*, IEEE.
- Bolaños-Torres MÁ, Torrealba-Meléndez R, Muñoz-Pacheco JM, *et al.*, 2018, Multiband flexible antenna for wearable personal communications. *Wirel Pers Commun*, 100(4):1753–1764.
- Ramos-Silva JN, Ramírez-García E, Alcántara-Gavilan BA, *et al.*, 2019, Design of a compact ultra wide band flexible antenna for personal mobile communications, in *2019 IEEE International Fall Meeting on Communications and Computing (ROCC-C)*, IEEE.
- Alharbi S, Shubair RM, Kiourti A, 2018, Flexible antennas for wearable applications: Recent advances and design challenges, in *AP-S International Symposium (Digest) (IEEE Antennas and Propagation Society)*.
- Zhang J, Song R, Zhao X, *et al.*, 2020, Flexible graphene-assembled film-based antenna for wireless wearable sensor with miniaturized size and high sensitivity. *ACS Omega*, 5(22):12937–12943.
- Lou Z, Wang LL, Shen GZ, 2018, Recent advances in smart wearable sensing systems. *Adv Mater Technol*, 3(12):1800444.
- Ometov A, Shubina V, Klus L, *et al.*, 2021, A survey on wearable technology: History, state-of-the-art and current challenges. *Comput Netw*, 93:108074.
- Sahnoun N, Messaoudene I, Denidni T, *et al.*, 2015, Integrated flexible UWB/NB antenna conformed on a cylindrical surface. *Prog Electromagn Res Lett*, 55:121–128.
- Hasan MR, Riheen MA, Sekhar P, *et al.*, 2020, Compact CPW-fed circular patch flexible antenna for super-wideband applications. *Iet Microw Antennas Propag*, 14(10):1069–1073.
- Kulkarni J, 2021, Wideband CPW-fed oval-shaped monopole antenna for wi-fi5 and wi-fi6 applications. *Prog Electromagn Res C*, 107:173–182.
- Zhong T, Jin N, Yuan W, *et al.*, 2019, Printable stretchable silver ink and application to printed RFID tags for wearable electronics. *Materials (Basel)*, 12(18):3036.
- Mirzaee M, Noghianian S, Wiest L, *et al.*, 2015, Developing flexible 3D printed antenna using conductive ABS materials, in *2015 IEEE International Symposium on Antennas and Propagation & USNC/URSI National Radio Science Meeting*, IEEE.
- Jilani SF, Abbasi QH, Alomainy A, 2018, Inkjet-printed millimetre-wave PET-based flexible antenna for 5G wireless applications, in *2018 IEEE MTT-S International Microwave Workshop Series on 5G Hardware and System Technologies (IMWS-5G)*, IEEE.
- Guo X, Hang Y, Xie Z, *et al.*, 2017, Flexible and wearable 2.45 GHz CPW-fed antenna using inkjet-printing of silver nanoparticles on pet substrate. *Microw Optical Technol Lett*, 59(1):204–208.
- Hettak K, Ross T, James R, *et al.*, 2013, Flexible polyethylene terephthalate-based inkjet printed CPW-fed monopole antenna for 60 GHz ISM applications, in *2013 European Microwave Conference*.
- Wagih M, Wei Y, Beeby S, 2018, Flexible 2.4 GHz node for body area networks with a compact high-gain planar antenna. *IEEE Antennas Wirel Propag Lett*, 18(1):49–53.
- Du ZM, Wong SW, Chen RS, *et al.*, 2022, Wide bandwidth ratio of 10-to-1 CPW-fed whip antenna with improved radiation patterns, in *IEEE Transactions on Antennas and Propagation*, IEEE.

25. Zou Q, Jiang S, 2021, A compact flexible fractal ultra-wideband antenna with band notch characteristic. *Microw Optical Technol Lett*, 63(3):895–901.
26. Yin B, Ye M, Yu Y, 2021, A novel compact wearable antenna design for ISM band. *Prog Electromag Res C*, 107:97–111.
27. Mattsson V, Ackermans L, Mandal B, *et al.*, 2021, MAS: Standalone microwave resonator to assess muscle quality. *Sensors (Basel)*, 21(16):5485.
28. Ashoke Raman K, 2018, Dynamics of simultaneously impinging drops on a dry surface: Role of inhomogeneous wettability and impact shape. *J Colloid Interface Sci*, 516:232–247.
29. Pu Z, Wang R, Wu J, *et al.*, 2016, A flexible electrochemical glucose sensor with composite nanostructured surface of the working electrode. *Sens Actuators B Chem*, 230: 801–809.